INVERSION OF EDDY CURRENT DATA AND THE RECONSTRUCTION OF FLAWS

PART 2: INVERSION OF DATA

L. David Sabbagh and Harold A. Sabbagh

Sabbagh Associates, Inc.
2634 Round Hill Lane
Bloomington, IN 47401

INTRODUCTION

Our multifrequency reconstruction algorithm is based on a rigorous electromagnetic model for eddy-current interactions with flaws in conducting tubes. The theoretical model was originally developed for nonferrous (stainless steel) tubes and was published in the IEEE Transactions on Magnetics [1]. The reader is encouraged to read [1] in order to understand the electromagnetic details of the model and algorithm; this will allow us to concentrate on applying the algorithm to laboratory reconstructions.

The electromagnetic analysis leads to certain integral equations which give the components of the perturbed magnetic induction field in terms of the two-dimensional Fourier transforms of the conductivity distribution of the anomalous region at each of N_r layers within the cylinder wall. The objective is to invert these equations, i.e., to determine the conductivity distribution, given the measured induction field as input data. Most of the experimental work has used the radial (r) component of the induction field as the data, but toward the end of the project we began to receive some axial (z) data. The z data has not been inverted yet.

The data is acquired by measuring the perturbed induction field at several frequencies, and then writing down an equation for each frequency. If there are N_f frequencies, then we arrive at a system of N_f equations in N_r unknowns, in each couple (m,h). In the laboratory experiments to be described later, we used 25 frequencies ($N_f = 25$), starting at 100 kHz and ending at 5 MHz. The number of layers, N_r, was equal to ten.

In our experiments we measure the radial component of the induction field as our input data. This introduces a slight complication in the inversion, because the transfer function that corresponds to the radial field has a zero on the axis (n,0) in Fourier space. This makes it impossible to invert the system. Therefore, we divide the transfer function by jh (analytically, of course) and integrate the data with respect to z. This produces a new, but equivalent, system that does allow inversion along the Fourier axis (m,0).

INVERSION VIA CONSTRAINED LEAST SQUARES (CLSP)

The unknown conductivities are normalized in physical space so that $-1 \leq \sigma_k(\phi,z) \leq 0$, where a value of -1 indicates the presence of an anomaly at (ϕ,z) and a value of 0 indicates the absence of an anomaly. In transform space this inequality translates into the constraint

$$|\tilde{\sigma}_k(m,h)| \leq |\tilde{\sigma}_k(0,0)|. \tag{1}$$

We define the support of a function as the region in space in which the function takes on nonzero values. In terms of the support the conductivity anomaly satisfies the following constraint in transform space

$$|\tilde{\sigma}_k(0,0)| \leq \textit{support}. \tag{2}$$

This, together with (1), implies that the unknown vector has a bounded norm

$$\|\tilde{\sigma}(m,h)\| \leq M, \tag{3}$$

where M is known whenever the support can be estimated.

In order to enforce the norm constraint, (3), on the least-squares solution we use a Levenberg-Marquardt parameter, together with a Newton iteration [2-3]. The constraints on each component of the solution vector, as in (2) and (3), can be satisfied by solving a Least Distance Problem [3-4].

EXTRAPOLATION IN THE FREQUENCY DOMAIN (EXFD)

The system matrix is a low-pass filter in the two-dimensional Fourier domain (m,h). This means that the matrix elements go to zero as (m,h) goes to infinity. Therefore, it is impossible (or at least extremely difficult) to invert the system to obtain the solution vector $\tilde{\sigma}_k(m,h)$ for large values of (m,h). It is usually desirable to have these high frequency components of $\tilde{\sigma}_k$ available, because they provide the resolution in the reconstructed conductivity anomaly. Therefore, some form of 'signal extrapolation' in the Fourier domain is necessary to recover the inherent resolution of the reconstructed signal. This is a common problem in deconvolution, and has received much attention in recent years in a variety of areas, ranging from image reconstruction and enhancement to 'super-resolving' radar antennas.

The possibility of signal extrapolation (which in mathematical terminology is called analytic continuation) is fully reported in [5].

EXPERIMENTAL RESULTS

Overview

There are two issues involved in the reporting of our experimental results: (1) how well does the model data agree with the laboratory data, both quantitatively and qualitatively, and (2) given the laboratory data, how well can the flaws be reconstructed.

The laboratory experiments were conducted on a 304 stainless steel tube whose outer diameter measured 7/8 inch, with a wall thickness of 0.048 inch. This is a standard tube for nuclear reactor applications, and has other applications as well. This class of stainless steel is

nominally nonmagnetic, and has an electrical conductivity of $1.4X10^6$ S/m. Defects of certain orientations and dimensions were machined into the tube by the process of electro-discharge machining (EDM).

The model and reconstruction algorithm are capable of predicting and utilizing the complete magnetic induction field vector, i.e., the radial (r), azimuthal (ϕ) and axial (z) components. These components are sensed by appropriately oriented microloop sensors.

In order to test the validity of the model, we generated model data for several flaws, in particular, flaws C and H for the radial sensor and flaw H for the axial sensor. We must remember that it is easy to generate the real and imaginary components of the model data at the various frequencies; however, since it is difficult to determine an exact 90° phase shift experimentally, the real and imaginary laboratory data are subject to phase errors as well as measurements errors.

Data Agreement for Radial Sensor

Since flaw C was used to calibrate the reconstruction technique, Figs. 1a and 1b show how well the model data and the laboratory data agree. We see that confidence about our radial model. By qualitative agreement, we mean that the peaks and valleys occur in the same places and have the same shapes; by quantitative agreement, we mean that the peak to peak values are in good agreement as are the rates of increase and decrease.

The agreement between the model data and the laboratory data for flaw H was similar to that of flaw C. We spot tested this agreement at several frequencies since we didn't need the model data at all 25 frequencies.

Integrated Data

As we mentioned previously, there is a need to integrate the laboratory data to produce a new, but equivalent, system so that we can invert the radial field at (m,0). Figures 2a and 2b show the agreement of the equivalent model data for flaw C and the integrated laboratory data for 300 kHz. One set of data must be multiplied by -1 to get the phase agreement.

Inversion of Radial Data

Since the resolution of the model and the laboratory data are different, we need to process the latter to make it consistent with the model so that the processed data can be presented to the inversion algorithm in the proper manner. The model has the following properties;

1. Its resolution is 1° in ϕ and 4 mils in z,
2. It is set up for 360 X 256 points at each of 25 frequencies,
3. The system matrix is even in m and odd in h; thus it is zero whenever h = 0.

The laboratory data has the following properties:

1. Its resolution is 4° in ϕ and 10.3125 mils in z,
2. It is set up for 24 X 100 data points at each of 25 frequencies.

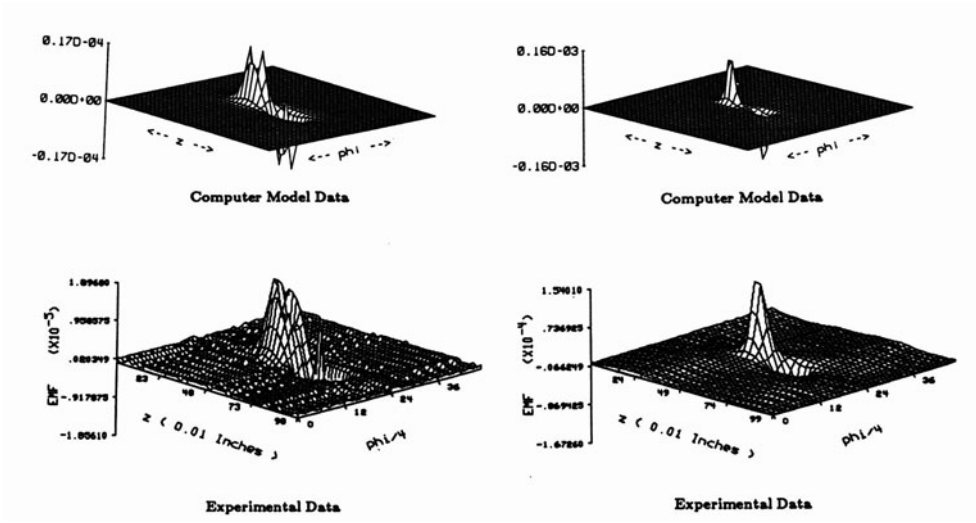

Fig. 1a. Real part of model data and laboratory at 500 kHz.

1b. Imag part of model data and laboratory at 500 kHz.

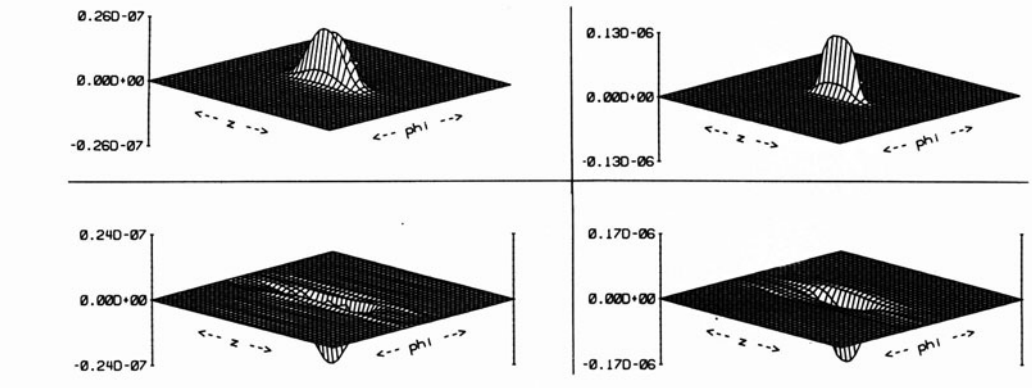

Fig. 2a. Real part of integrated model and laboratory data at 300 kHz.

2b. Imag part of integrated model and laboratory data at 300 kHz.

There are three steps in processing the radial laboratory data to make it consistent with the model. Step 1 is to interpolate from the laboratory resolution to the model resolution. We use a two dimensional quadratic interpolation scheme for this step. Step 2 is to extrapolate

so that the laboratory data from step 1 is extended to cover the same range as the model. We use an extrapolation technique that incorporates known information such as the bandwidth (generated from model) and the model data is zero at $(m,0),\forall m$. Step 3 is to integrate (with respect to the z direction) the resulting data from step 2 for the reasons stated before. We use a simple trapezoidal integration scheme.

The reconstruction algorithm consists of two parts as explained previously. The first part is to solve a CLSP for certain pairs (m,h). In these experiments, we considered $\{(m,h): 0 \leq m \leq 35, 0 \leq h \leq 15\}$. The processed laboratory data is then presented to CLSP and the output is presented to the second part algorithm, EXFD. EXFD is an iterative technique that switches between the frequency domain and the real domain and uses the FFT. In these experiments, EXFD was iterated ten times. The output of EXFD is then presented in a graphical manner so that the flaw can be visualized.

Figure 3a gives a gray scale visualization of the original flaw (OFC) at level 1. The gray scale visualization of OFC would be identical at levels 2, 3, and 4. Levels 5--10 should all be blank. Figures 3b, 3c, 3d and 3e give a gray scale visualization of the reconstructed flaw C (RFC) at levels 1, 2, 3 and 4, respectively. The gray scale visualization for RFC at levels 5--10 are all blank.

The gray scale visualization of levels 1--8 for the original flaw H (OFH) is the same as in Figure 3a since OFC and OFH differ only in their depth. Figures 4a, 4b, 4c, 4d and 4e give a gray scale visualization of the reconstructed flaw H (RFH) at levels 1, 2, 3, 4 and 5, respectively. Levels 6--10 are all blank.

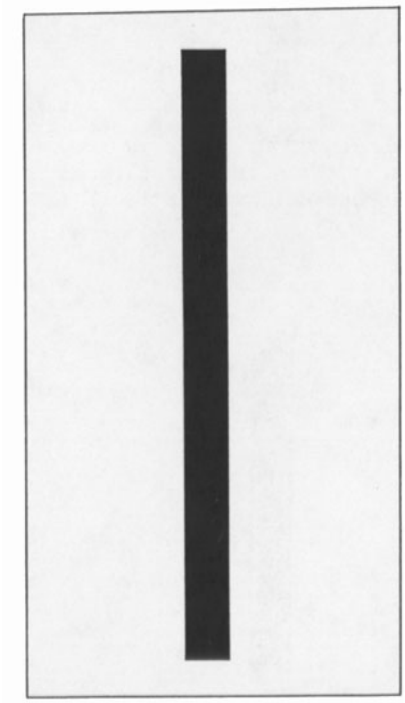

Fig. 3a. Gray scale image for flaw c at levels 1 - 4.

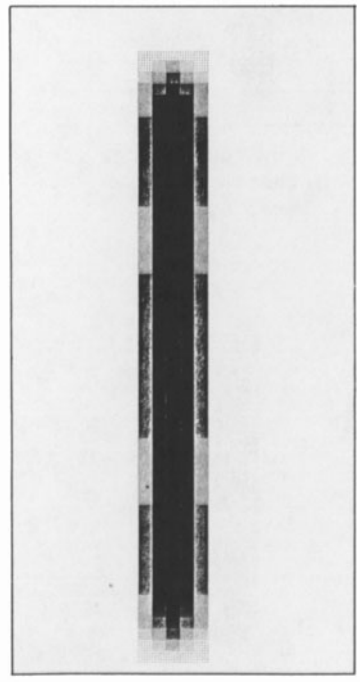

3b. Gray scale image for reconstructed flaw c at level 1.

Fig. 3c. Gray scale image for reconstructed flaw c at level 2.

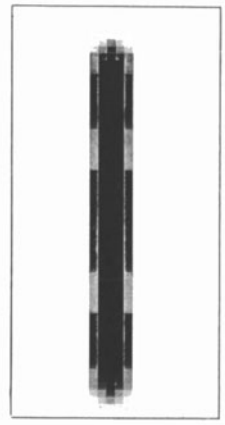

3d. Gray scale image for reconstructed flaw c at level 3.

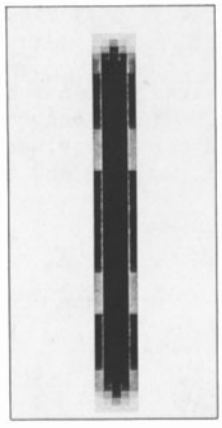

Fig. 3e. Gray scale image for reconstructed flaw c at level 4.

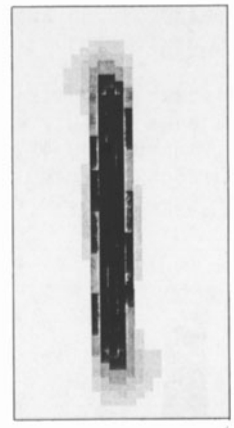

4a. Gray scale image for reconstructed flaw h at level 1.

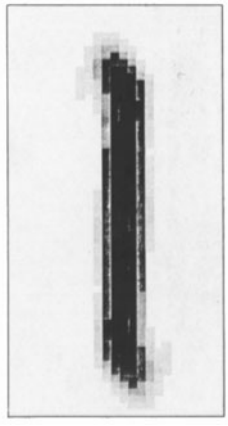

Fig. 4b. Gray scale image for reconstructed flaw h at level 2.

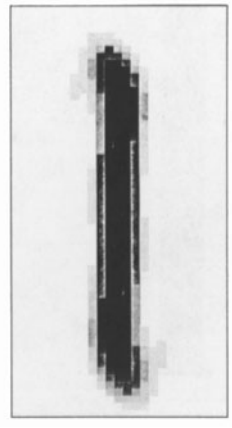

4c. Gray scale image for reconstructed flaw h at level 3.

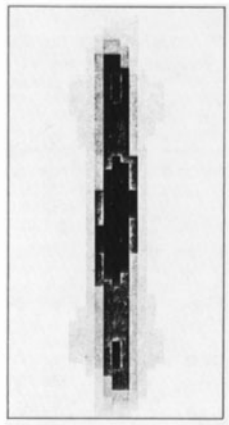

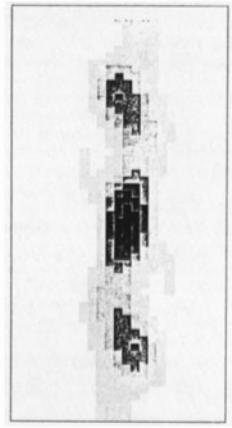

Fig. 4d. Gray scale image for reconstructed flaw h at level 4.

4e. Gray scale image for reconstructed flaw h at level 5.

Since flaw C was used to calibrate the model, we expect the results for its reconstruction to be quite good. It is possible that if we had kept more pairs (m,h) in CLSP and/or used more than 10 iterations in EXFD, the reconstruction of flaw C would have been even more faithful. However, there is a point where the computational results from CLSP are no longer valid due to the mathematical nature of inverse problems. Using more iterations, while time consuming on our conventional computer, would have resulted in a clearer picture.

The results from the reconstruction of flaw H were quite good through five levels. Again, due to the mathematical nature of inverse problems, the ability to get fine resolutions at depths is a difficult problem.

ACKNOWLEDGEMENT

This work was supported by the Department of Energy under Contract No. DE-AC02-83-ER80096 with Sabbagh Associates, Inc.

REFERENCES

1. H. A. Sabbagh and L. D. Sabbagh, "An Eddy-Current Model for Three-Dimensional Inversion", IEEE Transactions on Magnetics, Vol Mag-22, No. 4, (July 1986), 282-291.
2. Gene H. Golub and Charles F. Van Loan, Matrix Computations, (The Johns Hopkins University Press, Baltimore, MD).
3. Charles L. Lawson and Richard J. Hanson, Solving Lease Squares Problems, (Prentice Hall, Inc., Englewood Cliffs, NJ).
4. H. A. Sabbagh and L. D. Sabbagh, "Development of a System to Invert Eddy-Current Data and Reconstruct Flaws: Part 2, Multifrequency Approach", International Advances in Nondestructive Testing, 10, (1984).
5. L. D. Sabbagh, H. A. Sabbagh and J. S. Klopfenstein, "Image Enhancement Via Extrapolation Techniques: A Two Dimensional Iterative Scheme and A Direct Matrix Inversion Scheme", Review of Progress in Quantitative Nondestructive Evaluation 5A, ed. D. O. Thompson and D. E. Chimenti, (Plenum Press, New York, 1986), 473-483.

From the Floor: What dictated the choice of 10 levels in the r direction?

Mr. Sabbagh: The tube we were using is 48 mills, and so we chopped them 10 levels, which means each r level is approximately five mills.

From the Floor: I mean, does that choice enter into the compilation itself? I mean, is there a break-even point in subdividing?

Mr. Sabbagh: No. Just depends how fine you want to go in the r direction.

Now, by r equaling 10 levels, that means the least squares problems we solved for (each case) has 10 unknowns. Since we are working with 25 frequencies, I was solving a 25, actually, I made everything real, so that is doubled, thus we were solving a 50 by 10, least squares problem. But, no, it only depends how much resolution you want.

From the Floor: You might consider, say, if you decided to have 10 levels, to concentrate on the number of those close to the even diameter of your tube and make them a little bit more spaced out at the edge.

Mr. Sabbagh: That's high on our priority list of things to do. That's right. I agree.